Smart Mater. Struct. **9** (2000) 898–905. Printed in the UK PII: S0964-1726(00)17106-X

Design and development of a MEMS-IDT gyroscope

V K Varadan, W D Suh, P B Xavier, K A Jose and V V Varadan

Center for the Engineering of Electronic and Acoustic Materials and Devices,
Pennsylvania State University, University Park, PA 16802, USA

Received 21 July 2000, in final form 6 September 2000

Abstract. The design, development and performance evaluation of a novel radio frequency microelectromechanical systems (MEMS) gyroscope, based on a surface acoustic wave resonator (SAWR) and a surface acoustic wave sensor is presented in this paper. Most of the MEMS gyroscopes based on silicon vibratory structures that utilize the energy transfer between the two vibratory modes demand small fabrication tolerances to minimize signal output when there is no rotation (i.e. zero rate output). This 1 cm $\times$ 1 cm gyroscope operates based on the principle of a surface acoustic wave (SAW) on a piezoelectric substrate. The SAWR creates SAW standing waves within the cavity space between the interdigital transducers (IDTs). The particles at the anti-nodes of a standing wave experience large amplitudes of vibration perpendicular to the plane of the substrate, which serves as the reference vibrating motion for this gyroscope. A number of metallic dots (proof masses) are strategically positioned at the anti-node locations so that the effect of the Coriolis force due to rotation will amplify the magnitude of the SAW that is generated in the orthogonal direction. The performance of this 74.2 MHz MEMS-IDT gyroscope has been evaluated using rate table and geophone set-ups, indicating very high sensitivity and dynamic range, which is ideal for many of the commercial applications. Unlike other MEMS gyroscopes, this gyroscope has a planar configuration with no suspended resonating mechanical structures, thereby being inherently robust and shock resistant. In view of its one-layer planar configuration, this gyroscope can be implemented for applications requiring conformal mounting onto a surface of interest.

(Some figures in this article are in colour only in the electronic version; see www.iop.org)

1. Introduction

There have been an increasing number of applications for smaller and inexpensive gyroscopes or angular rate sensors due to the emergence of new consumer and automotive products that demand angular velocity information. Rotating wheel gyroscopes, fiber optic gyroscopes and laser gyroscopes have been extensively used for inertial navigation and guidance systems. However, they are bulky and expensive for newly emerging applications, despite their improved performance over many decades. Applications that require a smaller and cheaper gyroscope are found in automotive safety products (anti-skid systems, ABS, airbag systems), consumer products (3D pointer, camcorder, GPS, sports equipment), industrial products (robots, machine control, guided vehicles), medical products (wheel-chairs, surgical tools, body movement monitoring), and military products (smart ammunition, new weapon systems) [1].

Microsensors that consist of mechanical and electrical elements are commonly referred to as microelectromechanical systems (MEMS). Surface acoustic wave (SAW) devices, developed in the early 1960s, are considered to be the earliest type of MEMS because they utilize electrical signals to generate mechanical waves, and vice versa. MEMS sensors have received considerable attention over the last decade. They generally present the advantages of being lightweight, being small in size, having a low power consumption and low cost, due to standard IC fabrication techniques. With these benefits, research in MEMS gyroscopes has been accelerated and the performance of MEMS gyroscopes has been improved [2]. Most MEMS gyroscopes are silicon-based vibratory sensors, which utilize the energy transfer between two vibrating modes of a mechanical structure. Therefore, to achieve high sensitivity, it is imperative that the two oscillatory modes have to be easily transferable from each other with high Q when subjected to rotation [3–6]. Considerable design and fabrication efforts are also required for both the resonating structures to achieve a resolution of sub-degrees per second.

The demand for higher performance MEMS gyroscopes is steadily increasing. However, there is an inherent performance limitation for current MEMS gyroscopes due to their working principle, which is based on the vibration of a suspended mechanical structure, i.e. comb structure, beam, disk, or ring structures. It is often difficult and expensive to fabricate mechanical structures with matching resonant frequencies of the two modes. The cost of final products may increase due to the electronics required to control and detect the status of the resonating structure. In addition, the suspended vibrating mechanical structure becomes sensitive

0964-1726/00/060898+08$30.00

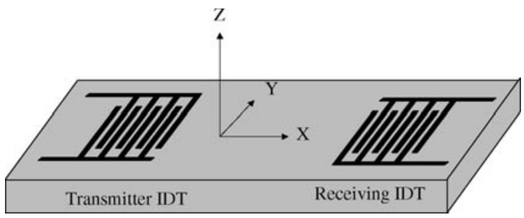

Figure 1. Typical SAW sensor.

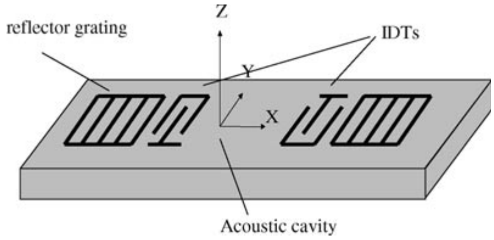

Figure 2. Typical SAW resonator.

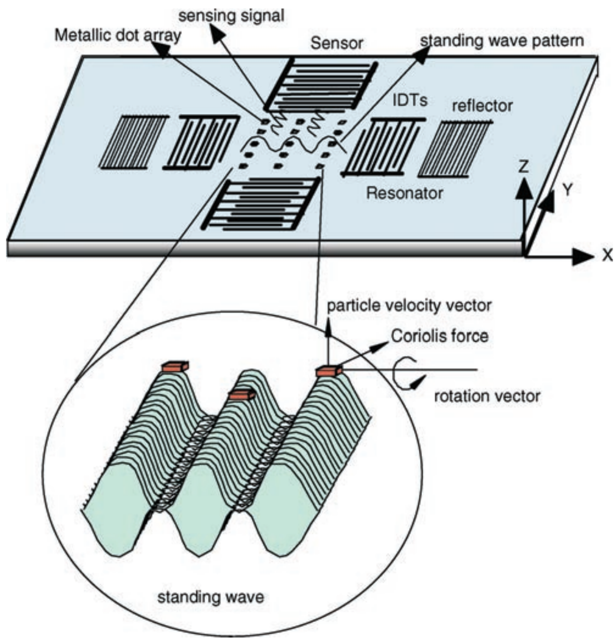

Figure 3. Working principle of the MEMS SAW gyroscope.

to external shock and vibration because the structure cannot be rigidly attached to the substrate for its resonant vibration. This limits its application range and performance.

The gyroscope presented in this paper can overcome those limitations since this gyroscope has no suspended mechanical structure. The gyroscope constructed is based on the combination of a surface acoustic wave resonator (SAWR) and a surface acoustic wave sensor (SAWS), which operates at the Rayleigh mode [7–9]. The Rayleigh wave is a SAW which has its energy concentrated within one wavelength of the substrate surface. The displacement of particles near the surface due to the Rayleigh wave has an out-of-surface motion that traces an elliptical path [10]. The Rayleigh wave can be generated at the surface of piezoelectric material by applying a voltage to an interdigital transducer (IDT) patterned on the substrate [11].

This SAW gyroscope works on the principle of particle vibration of the substrate due to the standing Rayleigh waves created by the SAWR; as such no suspended mechanical structure is required for the reference vibration. Therefore, it is more resistant to external shock and vibration. In addition to these advantages, this gyroscope only requires one or two lithography and metallization steps for fabrication using standard IC fabrication techniques. This will clearly translate to a reduction in cost of development on a large scale. Lao [12] and Kurosawa *et al* [13] proposed a gyroscope design, which is based on SAWs, to measure the angular rate. However, to-date and to the best of our knowledge there are no conclusive experimental results available. This paper presents the proof of concept through fabrication and performance evaluation of the gyroscope.

2. Design principle

The SAW device has been used as a sensor, filter and oscillator [7–10]. Figure 1 shows a typical SAW delay line for which one of the IDTs acts as a transmitter that converts the applied voltage variation into acoustic waves. The other IDT receives these acoustic waves and converts them back to an output voltage. This reciprocity allows IDTs to be used either as a SAW transmitter or a receiver. For this gyroscope, the SAW delay line is used as a receiver for sensing the acoustic waves created by the Coriolis effect when this gyroscope is subjected to a rotation.

SAWRs have been extensively used as stable frequency oscillators and resonant filters due to their ruggedness and small size compared to the resonators based on bulk material vibration [7, 8]. The SAWRs are used as the stable reference vibration source for this gyroscope since any mechanical gyroscope must have a stable reference vibrating motion ($\boldsymbol{V}$) of a mass (m) such that the angular rotation ($\boldsymbol{\Omega}$) perpendicular to the reference motion ($\boldsymbol{V}$) would cause Coriolis forces at the frequency of the reference motion. Therefore, the effect of the Coriolis force ($\boldsymbol{F} = 2m\boldsymbol{V} \times \boldsymbol{\Omega}$) can be a measure of the rotation rate. The methods of sensing the Coriolis effect are usually capacitive or piezoelectric. This SAW gyroscope utilizes the piezoelectric effect through IDT's as explained earlier.

This SAW gyroscope is an integration of a SAWS (figure 1) and a SAWR (figure 2) where the SAWR is required for exciting the stable reference vibrating motion and the SAWS is required for the detection of the Coriolis effect. As shown in figure 3, this gyroscope consists of IDTs, reflectors and a metallic dot array within the cavity. The IDTs, reflectors and metallic dot array are fabricated through microfabrication techniques on the surface of a piezoelectric substrate, 128° YX $LiNbO_3$. The resonator IDTs create SAWs that propagate back and forth between the reflectors and form a standing wave pattern within the cavity due to the collective reflection from the reflectors. SAW reflection from individual metal strips adds in phase if the reflector periodicity is equal to half a wavelength [7, 8]. For the established standing wave pattern in the cavity as explained in figure 3, a typical substrate particle at the nodes of a standing wave has no amplitude of deformation in the Z-direction. However, at or near the anti-nodes of the standing wave pattern, such particles experience larger amplitudes of vibration in the Z-direction, which serves as the reference vibrating motion for this gyroscope. In order to acoustically amplify the magnitude of the Coriolis force in phase, metallic dots (proof mass) are positioned strategically at the anti-node locations. The rotation (Ω, x-direction) perpendicular to the velocity ($\boldsymbol{V}$ in $\pm z$-direction) of the oscillating masses (m) produces Coriolis force ($\boldsymbol{F} = 2m\boldsymbol{V} \times \Omega$, in $\pm y$-direction) in the direction perpendicular to the both vectors as shown in figure 3. This Coriolis force establishes a SAW in the y-direction of the same frequency as the reference oscillation. The metallic dot array is placed along the y-direction such that the SAW due to the Coriolis forces adds up coherently. The generated SAW is then sensed by the sensing IDTs placed in the y-direction.

The operating frequency of the device is determined by the separation between the reflector gratings, periodicity of reflectors, and IDTs. The separation between reflectors was chosen as an integral number of half-wavelengths such that standing waves are created between both reflectors. The periodicity of IDT was chosen as a half-wavelength ($\lambda/2$) of the SAW. Therefore, for a given material, the SAW velocity in the material and the desired operating frequency, f_o, define the periodicity of the IDT. The SAW velocity can be found from elsewhere or from the theoretical calculation for a free surface condition with a given material and a coordinate system [10, 14, 15]. However, for this gyroscope, the effective SAW velocities were experimentally measured in the X- and Y-directions, because the device utilizes wave propagation in these directions and the effect of the metallic dot array on the velocities in both directions is not fully known. To measure the effective velocities of the waves in both directions, two narrow-band IDT sets with the same periodicity were placed in the X- and Y-directions including the dot array in the middle. The wave velocity is different in the X- and Y-directions due to the anisotropy of 128° YX $LiNbO_3$. Hence, the response measured using IDTs in the X- and Y-directions were different for the same periodicity of these IDT sets, and the velocities of both directions were measured as 3961 m s^{-1} and 3656 m s^{-1}, respectively. The errors between published values (3980–4000 m s^{-1}) and the experimental results are mainly due to the effect of metallization and the metallic dot array. The width of the IDT fingers and its spacing for the SAW gyroscope were determined according to the velocities 3961 m s^{-1} and 3656 m s^{-1} in the X- and Y-directions, respectively.

To reduce the effect of the metallic dot array inside the SAWR, the size of each dot in the array was chosen such that they are sufficiently smaller than the wavelength in both directions. Since the amplitudes of the standing waves are dependent on material damping and electromechanical transduction losses, the transmitting and sensing IDTs are placed such that they are located at the standing wave maxima in order to reduce the transduction loss. To obtain good resonator performance with this high-coupling-coefficient substrate, the aperture of the IDTs and number of IDT fingers were minimized, but were large enough to avoid acoustic beam diffraction. Also, larger spacing between the IDTs was chosen, compared to conventional resonators, since the electromagnetic coupling between IDTs has to be avoided, and enough metallic dots should be accommodated within the cavity for the Coriolis effect.

The number and aperture of IDTs, the electromechanical coupling coefficient, and the dielectric permittivity of the substrate determine the electrical impedance of the gyroscope. Thus, the spacing, aperture, and number of IDTs were chosen as a compromise between the different requirements. Also, the impedance matching during the packaging was performed using series inductors or a transformer since this gyroscope is largely capacitive due to the arrangement of IDT fingers.

The initial design of this SAW gyroscope was incorporated from the separate study of both a resonator and a delay line. It is imperative to know the characteristic of impedance, admittance, bandwidth, and the sensitivity of the sensing IDTs near the operating frequency of the SAW resonator, because the sensing IDTs have to be designed such that they efficiently pick up the SAWs generated from the Coriolis force. It is assumed that the optimal design of the delay line and resonator will translate to an efficient gyroscope design, if the effect of the metallic dot array on the resonator is minimal. Thus, it is important to know the change in resonator characteristics due to the metallic dot array within the cavity space.

The sensing IDTs of the gyroscope, which are positioned perpendicular to the resonator, were designed through a typical SAW delay line and filter transfer function computation [16]. The response of the delay line in the frequency domain can be obtained from the transfer function as shown below.

The radiation conductance and susceptance of each IDT can be written as [16]

$$G_a = 8N_p^2 K^2 f_o C_s \left| \frac{\sin[N_p\pi(f - f_o)/f_o]}{N_p\pi(f - f_o)/f_o} \right|^2 \tag{1}$$

$$\begin{aligned} B_a = {} & 8N_p^2 K^2 f_o C_s |(\sin[N_p\pi(f - f_o)/f_o] \\ & -[N_p\pi(f - f_o)/f_o])([N_p\pi(f - f_o)/f_o]^2)^{-1}| \end{aligned} \tag{2}$$

where N_p is the number of fingers in each IDT, K^2 is the coupling coefficient, and C_s is capacitance per finger pair.

The input and output admittance of each IDT are given by

$$y_{ii} = G_a + \mathrm{i}(B_a + \omega C_T) \qquad \text{for } \omega \neq \omega_o \tag{3}$$

$$y_{ii} = G_a + \mathrm{i}(\omega C_T) \qquad \text{for } \omega = \omega_o \tag{4}$$

where C_T is total capacitance of IDT.

The transfer admittance can be as follows

$$y_{ij} = G_o N M \mathrm{e}^{-\mathrm{i}\omega\tau_o} \qquad \text{for } \omega = \omega_o \tag{5}$$

$$\begin{aligned} y_{ij} = {} & G_o N M \frac{\sin(\pi N(\omega - \omega_o)/(2\omega_o))}{\pi N(\omega - \omega_o)/(2\omega_o)} \\ & \times \frac{\sin(\pi M(\omega - \omega_o)/(2\omega_o))}{\pi M(\omega - \omega_o)/(2\omega_o)} \mathrm{e}^{-\mathrm{i}\omega\tau_o} \qquad \text{for } \omega \neq \omega_o \end{aligned} \tag{6}$$

where N and M are the number of finger pairs in the input and output IDTs.

The transfer function is can be written as

$$A = \frac{(y_1 + y_2)y_{12}}{y_{12}^2 - (y_1 + y_{11}) - (y_2 + y_{22})} \tag{7}$$

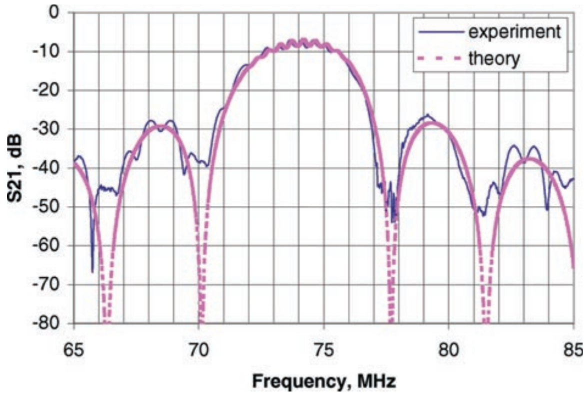

Figure 4. Computed and measured performance of the SAW delay line.

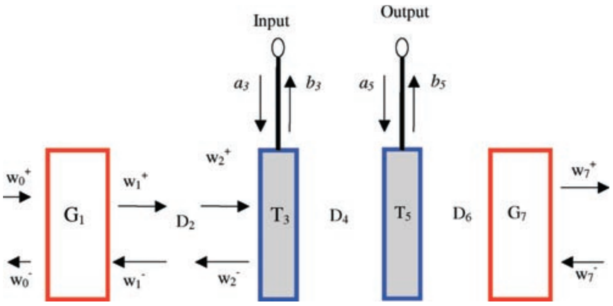

Figure 5. Schematic matrix representation of a SAWR.

where y_1 and y_2 are the source and load admittance and y_{12}, y_{11}, and y_{22} are the transfer, input, and output admittances of the IDTs, respectively.

Figure 4 shows the theoretical and experimental results of the SAW delay line. The prediction of the delay line response was quite satisfactory in terms of its bandwidth and insertion loss, although a slight downshift of the operating frequency and insertion loss exist.

The resonator response was studied using the coupling-of-modes (COM) theory [17, 18]. As shown in figure 5, the two-port resonator can be represented in terms of its component matrices as shown below. The G matrix represents SAW reflectors, the τ matrix represents the relation between electric and acoustic parameters and the D matrix represents the acoustic space between the IDTs and the reflectors. The boundary conditions can be applied, assuming that there are no incoming waves from the outsides of reflectors and the impedances are matched at electrical terminals. Then, the first-order response of the two-port resonator can be obtained by solving the following equations:

$$[W_5] = [D_6][G_7][W_7]. \tag{8}$$

By applying the ideal boundary conditions mentioned above,

$$\left\{ \begin{matrix} 0 \\ w_0^- \end{matrix} \right\} = [M] \left\{ \begin{matrix} w_7^- \\ 0 \end{matrix} \right\} + a_3[G_1][D_2][\tau_3]. \tag{9}$$

The output voltage from the IDT can be written as

$$V_{out} = b_5 = [\tau'][W_5]. \tag{10}$$

The transfer functions of the IDTs were evaluated and the experimental result was compared with the theoretical predictions using COM theory. Figure 6 shows the comparison between the theoretical predictions and the experimental results of the resonator. The errors in resonant frequency and insertion loss were caused by the existence of the metallic dot array and minor impedance mismatches between the electrical and acoustic ports.

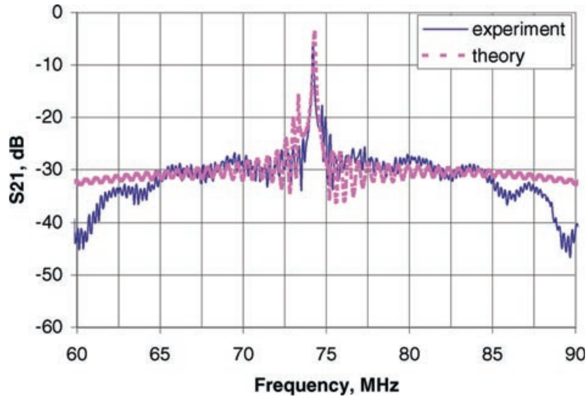

Figure 6. Computed and measured performance of the SAWR.

Figure 7. Measured response of the gyroscope using the rate table.

3. Fabrication, packaging and testing

The gyroscopes were fabricated at the nanofabrication facility of Penn State University, by the both liftoff technique and reactive ion etching (RIE). The liftoff technique was adequate for 75 MHz gyroscopes that have a minimum feature size of about 6 μm. For the same type of photoresist used to establish the pattern of the gyroscope, a positive or negative mask is used for the RIE and liftoff process, respectively. An initial layer of chromium is deposited as an adhesion promoter on the lithium niobate substrate prior to coating with an additional layer of gold. The processed wafers were subsequently diced and the individual devices were mounted on a microcircuit package for testing purposes. The gyroscopes were wire-bonded and sealed with a conductor cap to isolate them from environmental noise. The packaged device was then mounted onto a designed circuit board, which contains an onboard oscillator circuitry. It should be noted that this packaged gyroscope was not hermetically sealed in the first instance. The initial testing of the device was performed using a HP 8510C network analyzer.

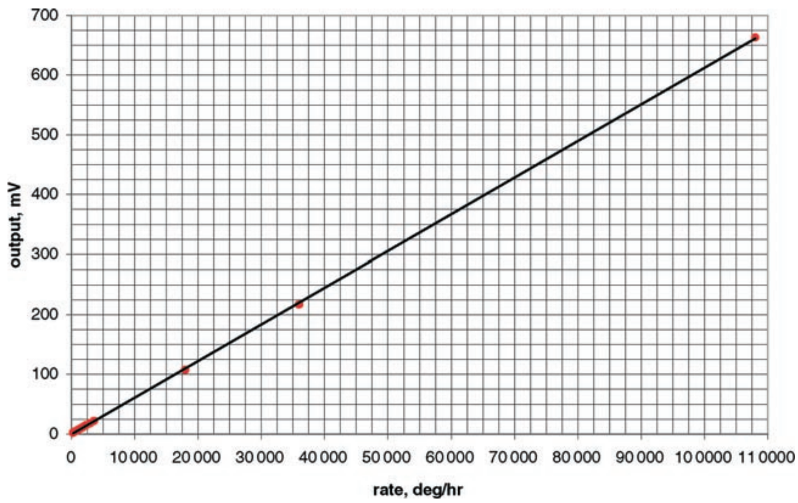

Figure 8. Measured response of the BEI gyroscope using the rate table.

The response of the SAW gyroscope was evaluated using a rate table set-up and a geophone set-up. The gyroscope signal due to the Coriolis force propagates towards the SAWS, which comes out along with the diffracted signals from the resonator. It could be possible to separate the coupled signal from the gyroscope signal using phase-locked detection. The output from the gyroscope is connected to the HP dynamic signal analyzer through a radio frequency (RF) lock-in amplifier. The initial measurements of the gyroscope were made using a rate table for constant oscillations. The gyroscope is fixed onto a rate table and, giving constant frequency, drives the rate table in oscillations and the output from the gyroscope is measured. The amplitude and the frequency of the driving signal controls the amplitude of the oscillations of the table, which in turn varies the rotation rate. Figure 7 shows the measured output voltage from the SAW gyroscope for different rotation rates. Due to the difficulties in driving the rate table at lower rates, we further measured the sensitivity of the gyroscope using a geophone–pendulum set-up. Two geophones are arranged at the opposite end of a rectangular platform that serves to set up horizontal oscillations and another pair of geophones will pick up the table oscillations. The platform is suspended at its four corners using flexible strings. The gyroscope was mounted at the center of the horizontal platform by aligning its X-axis such that it can oscillate about the vertical axis of the platform. The geophones are utilized to generate and to sense the rotation of the pendulum while the output signal from the gyroscope is detected through a lock-in amplifier at the excitation frequency. Adjusting the amplitude of the driving signal can control the rate of oscillation of the pendulum. The pendulum is calibrated for rotation rate using a BEI gyroscope (Gyrochip), whose output voltage is measured and calibrated using a rate table. The BEI gyroscope is mounted on a rate table (Ideal Aerosmith, PA) and its response for different rotation rates is evaluated, as shown in figure 8. The same gyroscope is then fixed on a geophone–pendulum set-up and its response is measured for the different excitation frequencies of the geophone. The voltage level of the excitation signal is changed so that the table will oscillate at different amplitudes, which are directly related to different rotation rates. Figure 9(a) shows the measured response of the SAW gyroscope at 20 Hz excitation and 3 V for an averaging factor of 12. The measurements were taken using the time averaging of the signal analyzer, which gives a good signal-to-noise ratio. The response from the BEI gyroscope is measured for the same excitation voltage, which is then calibrated to the rotation rate using the voltage response from the rate table measurements. From the output voltage level of the BEI gyroscope, it can be seen that the table oscillation at 3 V excitation is $950^\circ\ h^{-1}$. Figure 10 shows the output of the SAW gyroscope and BEI gyroscope for a 20 HZ, 2 V excitation, which corresponds to a rotation rate of $625^\circ\ h^{-1}$. It can be clearly seen from figures 9 and 10 that the excitation voltage of the geophone directly translates to the different rotation rates of the table. The response of the SAW gyroscope was measured and compared with that from the reference BEI gyroscope to validate the gyroscope signal for different excitation voltages and is calibrated to the rotation rate of the table. Figure 11 shows the measured response of the SAW gyroscope for different rotation rates. This initial measurement demonstrates the viability of using a SAW gyroscope to measure rotation rates. Because the proper packaging was not done at this stage, the measurements make it difficult to determine the dynamic range and resolution. However, with proper packaging it should be able to measure low rotation rates.

4. Results and discussion

In view of the working principle discussed above, any piezoelectric material such as lithium niobate, lithium tantalite, or quartz could be used as a substrate. In order to integrate easily with solid-state electronics, silicon with ZnO film or an Si/diamond/ZnO combination could also be used. However, to prove the concept of the SAW gyroscope, a low-loss material with a high electromechanical coupling coefficient was chosen for the present study. For efficient generation and detection of SAWs through IDTs, 128° YX $LiNbO_3$ crystal wafer was chosen as the substrate since it is known to excite fewer bulk waves and has a very high electromechanical coupling coefficient. The metallic dot array within the cavity of resonator would partially act as a mass-loading element and a piezoelectric shortening

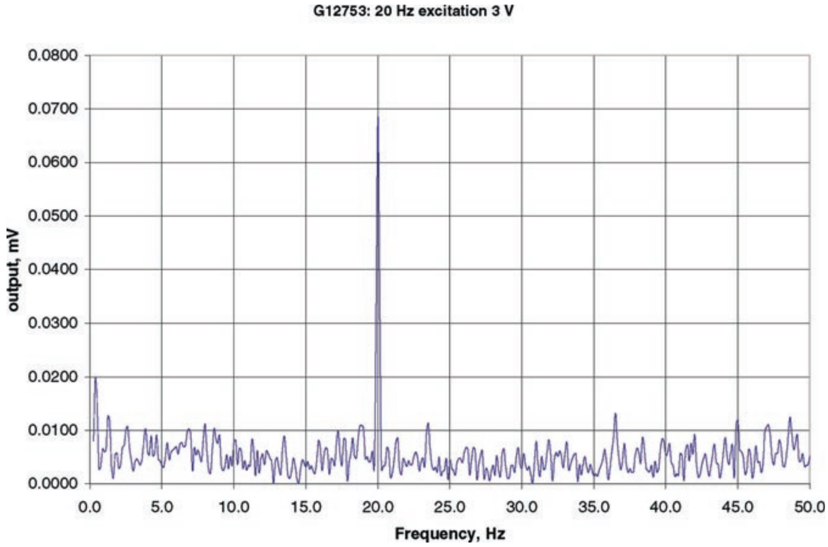

(*a*)

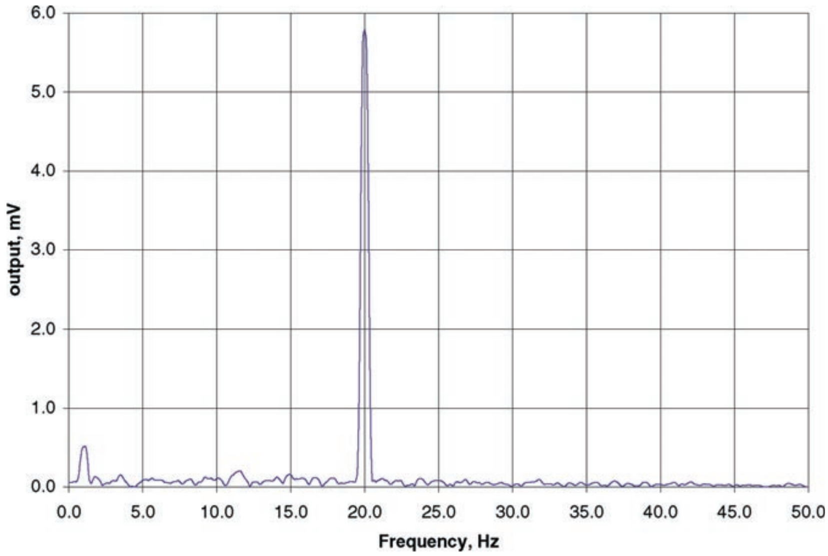

(*b*)

Figure 9. (*a*) Measured response of the SAW gyroscope on the geophone set-up for 20 Hz excitation. (*b*) Measured response of the BEI gyroscope for 20 Hz, 3 V excitation.

element, which creates impedance mismatch, hence the reflection of the SAW. To decrease the mass loading effect, the thickness of the material was kept to be less than 1% of a wavelength.

Several different designs of this gyroscope were explored, corresponding to different resonator designs. In particular, a two-port resonator configuration, which has been the subject of discussion so far, was chosen since its impedance variation is less than that of a one-port resonator. The feedback loop through the oscillator between the transmitting IDT and the receiving IDT also helped in maintaining the stable operation of the resonator. For the reflector strips of the resonators, open metal strips and shorted metal strips were investigated, and the resonators with shorted metal strips outperform the others due to different reflection mechanisms of the strips of this high-coupling-coefficient substrate. Reflection effect due to piezoelectric shortening is usually predominant for materials like $LiNbO_3$.

The test results for the gyroscope with the one-port resonator are poor since the transmitter IDT is located in the middle of the cavity and interferes with the generation of the Coriolis force. The best results are obtained for the gyroscope based on the two-port configuration with shorted reflectors. To achieve higher loaded Q-factor, vacuum packaging should be employed to decrease the loading from the atmosphere. The packaging is a very important part of realizing this gyroscope. For high-frequency operations, the frequency stability and sensitivity of gyroscope should be protected from any environmental effects through proper packaging. Laser trimming at sub-micrometer resolution would help for greater accuracy and phase linearity of the oscillation circuits.

5. Conclusions

In this paper, the design, fabrication, and performance evaluation of a microgyroscope based on SAWR and a

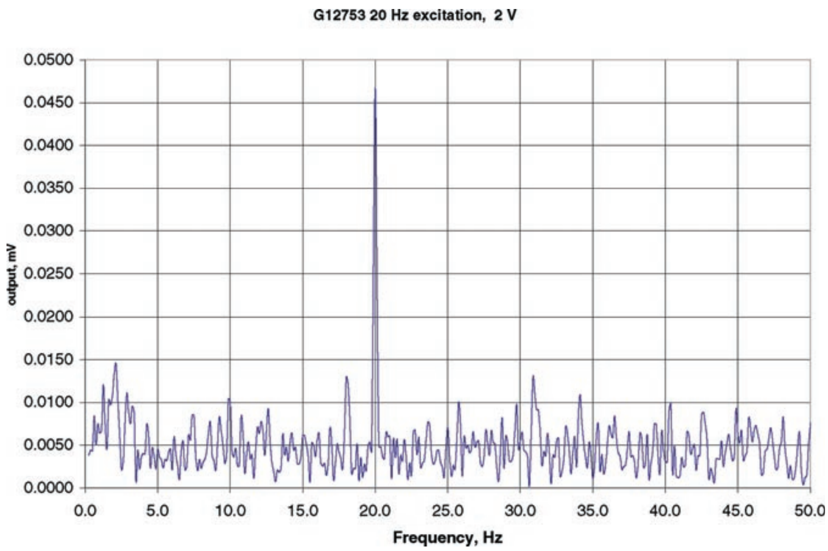

(*a*)

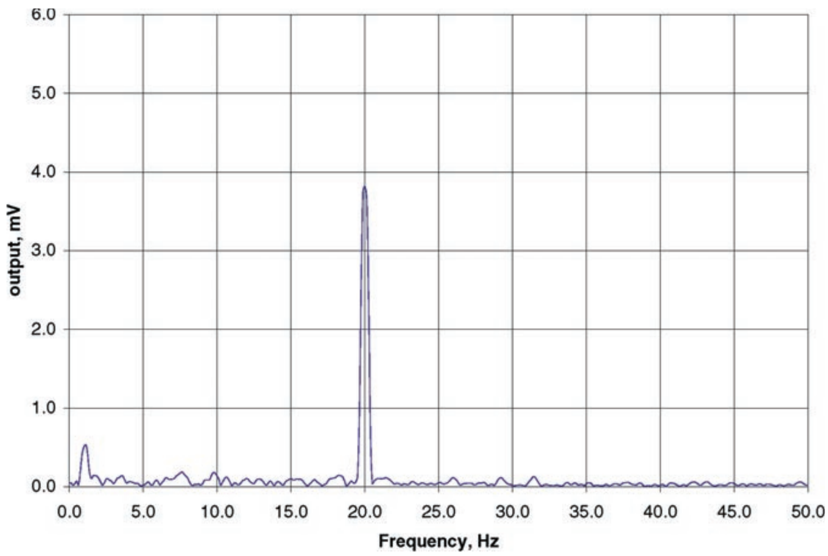

(*b*)

Figure 10. (*a*) Measured response of the SAW gyroscope for 20 Hz, 2 V excitation. (*b*) Measured response of BEI gyroscope for 20 Hz, 2 V excitation.

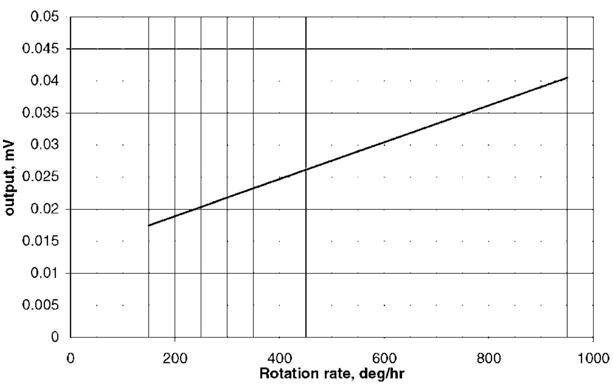

Figure 11. Response of SAW gyroscope on geophone set-up after calibration using BEI gyroscope.

SAWS were presented. This gyroscope possesses inherent ruggedness to external shock and vibration due to the absence of any suspended mechanical vibratory elements. This preliminary result indicates that this gyroscope has application potential not only for commercial grade products, but also in tactical and inertial grade components.

The importance of packaging could not be over emphasized, since the device operates in the high-frequency range compared to most common MEMS gyroscopes, which operate in kilohertz range. This high-frequency operation accounts for the high-resolution performance. However, acoustic attenuation at high frequencies should be minimized and noise should be reduced through the proper design, shielding, and packaging.

The authors are currently working towards an accurate model based on the equivalent circuit for this SAW gyroscope, which should give a more accurate prediction on how the gyroscope response scales with the frequency of operation. For the higher-frequency gyroscopes, RIE produced the features of better line definition despite the small feature sizes. This is especially critical to performance when the feature sizes approach 1 μm for higher-frequency devices. The authors are developing a wireless 915 MHz SAW gyroscope based on the presented concept combined with previous work on a wireless strain sensor [19, 20]. To date, a 400 MHz gyroscope has been successfully fabricated using RIE, and a 915 MHz gyroscope has been fabricated to be integrated with an antenna system for wireless applications. These will be discussed in a follow-up paper.

References

[1] Soderkvist J 1994 Micromachined gyroscopes *Sensors Actuators* A **43** 65–71

[2] Yazdi N, Ayazi F and Najafi K 1998 Micromachined inertial sensors *Proc. IEEE* **86** 1640–58

[3] Juneau T and Pisano A P 1996 Micromachined dual input axis angular rate sensor *Tech. Digest Solid-State Sensor and Actuator Workshop (Hilton Head Island, SC)* pp 299–302

[4] Tanaka K *et al* 1995 A micromachined vibrating gyroscope *Sensors Actuators* A **50** 111–15

[5] Park K Y *et al* 1997 Laterally self-oscillated and forced-balanced micro vibratory gyroscope packaged in vacuum package with a conditioning ASIC *Proc. SPIE* **3242** 76–85

[6] Putty M P and Najafi K 1994 A micromachined vibrating ring gyroscope *Tech. Digest Solid-State Sensor and Actuator Workshop (Hilton Head Island, SC, June 1994)* pp 213–20

[7] Bell D T Jr and Li C M 1976 Surface acoustic wave resonators *Proc. IEEE* **64** 711–21

[8] Staples E J 1974 UHF surface acoustic wave resonators *Ultrasonics Symp. Proc.* (Piscataway, NJ: IEEE) pp 245–52

[9] White R M 1985 Surface acoustic wave sensors *Proc. IEEE Ultrasonics Symp.* pp 490–4

[10] Slobodnik A J 1976 Surface acoustic waves and SAW materials *Proc. IEEE* **64** 581–95

[11] White R M and Voltmer F W 1965 Direct piezoelectric coupling to surface acoustic waves *Appl. Phys. Lett.* **7** 314–16

[12] Lao B Y 1980 Gyroscopic effect in surface acoustic waves *IEEE Ultrasonics Symp.* pp 687–90

[13] Kurosawa M *et al* 1997 A surface acoustic wave gyro sensor *Int. Conf. Solid-State Sensors and Actuators (Chicago, June 16–19, 1997)* pp 863–6

[14] Campbell J J and Jones W R 1968 A method for estimating optimal crystal cuts and propagation directions for excitation of piezoelectric surface waves *IEEE Trans. Sonics Ultrasonics* **15** 209–17

[15] Auld B A 1990 *Acoustic Fields and Waves in Solids* 2nd edn (Malabar, FL: Krieger)

[16] Soluch W 1997 Design of SAW delay lines for sensors *11th Eur. Conf. on Solid State Transducers (Warsaw, Poland)* pp 797–800

[17] Haus H and Wright P V 1980 The analyses of grating structures by coupling-of-modes theory *IEEE Utrasonics Symp.* vol 1, pp 277–81

[18] Cross P S and Schmidt R V 1977 Coupled surface acoustic wave resonator *Bell System Tech. J.* **56** 1447–81

[19] Varadan V V, Varadan V K, Bao X, Ramanathan S and Piscotty D 1997 Wireless passive IDT strain microsensor *Smart Mater. Struct.* **6** 745–51

[20] Varadan V K, Xavier P B, Suh W D, Kollakompil J A and Varadan V V, Microelectromechanical gyroscope US Patent filing No 09/594370